
PERGAMON

Journal of the Mechanics and Physics of Solids
50 (2002) 81–99

JOURNAL OF THE
MECHANICS AND
PHYSICS OF SOLIDS

www.elsevier.com/locate/jmps

A finite deformation theory of strain gradient plasticity

K.C. Hwang[a], H. Jiang[a], Y. Huang[b,*], H. Gao[c], N. Hu[a]

[a] *Failure Mechanics Laboratory, Department of Engineering Mechanics, Tsinghua University, Beijing 100084, China*
[b] *Department of Mechanical and Industrial Engineering, University of Illinois, Urbana, IL 61801, USA*
[c] *Division of Mechanics and Computation, Stanford University, Palo Alto, CA 94305, USA*

Received 4 May 2000; received in revised form 17 February 2001; accepted 20 February 2001

Abstract

Plastic deformation exhibits strong size dependence at the micron scale, as observed in micro-torsion, bending, and indentation experiments. Classical plasticity theories, which possess no internal material lengths, cannot explain this size dependence. Based on dislocation mechanics, strain gradient plasticity theories have been developed for micron-scale applications. These theories, however, have been limited to infinitesimal deformation, even though the micro-scale experiments involve rather large strains and rotations. In this paper, we propose a finite deformation theory of strain gradient plasticity. The kinematics relations (including strain gradients), equilibrium equations, and constitutive laws are expressed in the reference configuration. The finite deformation strain gradient theory is used to model micro-indentation with results agreeing very well with the experimental data. We show that the finite deformation effect is not very significant for modeling micro-indentation experiments.

Keywords: Finite deformation; Strain gradient plasticity; Micro-indentation

1. Introduction

Recent experiments have repeatedly shown that the material behaviour displays strong size dependence at the micron or sub-micron scales. For example, in micro-indentation and nano-indentation hardness experiments, the measured indentation hardness increases by a factor of 2 or even 3 as the depth of indentation decreases to microns or sub-microns (Nix, 1989; De Guzman et al., 1993; Stelmashenko et al., 1993; Atkinson, 1995; Ma and Clarke, 1995; Poole et al., 1996; McElhaney et al., 1998; Suresh et al.,

* Corresponding author. Tel.: +1-217-265-5072; fax: +1-217-244-6534.
E-mail address: huang9@uiuc.edu (Y. Huang).

0022-5096/01/$ - see front matter
PII: S0022-5096(01)00020-5

1999). Fleck et al. (1994) have observed in micro-torsion of thin copper wires that the scaled shear strength increases by a factor of 3 as the wire diameter decreases from 170 to 12 μm. Stolken and Evans (1998) have found similar strength increase in micro-bending of thin nickel foils as the foil thickness decreases from 50 to 12.5 μm. In particle-reinforced metal-matrix composites, Lloyd (1994) has observed substantial increase in work hardening as the particle diameter is reduced from 16 to 7.5 μm at a fixed particle volume fraction of 15%. Nan and Clarke (1996) have made similar observations. Classical plasticity theories, however, cannot explain this size dependence observed at the micron or sub-micron scale because their constitutive models possess no internal material lengths. At the micron scale, however, there are still hundreds of dislocations such that there should be a continuum plasticity theory (but not classical plasticity) that can describe the collective behavior of these dislocations.

For this reason, strain gradient plasticity theories have been developed and are intended for applications to materials and structures whose dimension controlling plastic deformation falls roughly within a range from a tenth of a micron to 10 μm (e.g., Fleck and Hutchinson, 1993, 1997; Fleck et al.,1994; Gao et al., 1999; Acharya and Bassani, 2000; Acharya and Beaudoi, 2000; Huang et al., 2000a, b; Dai and Parks, 2001). Strain gradients have been introduced in the constitutive model. From dimensional considerations, the internal material length parameters have been introduced to scale the strain gradients and these length parameters are determined to be on the order of microns or sub-microns either from the aforementioned micro-scale experiments of indentation, torsion and bending, or from the dislocation models (Nix and Gao, 1998).

The higher-order stresses serve as the work conjugates of strain gradients in the theories of Fleck and Hutchinson (1997), Gao et al. (1999), and Huang et al. (2000a, b). These theories have shown reasonable agreement with the micro-scale experiments. However, they are limited to infinitesimal deformation, while the aforementioned micro-scale experiments involve rather large strains and rotations. For example, the surface strain in the micro-torsion experiment exceeded 100% (Fleck et al., 1994), while the strain near the indenter tip was also very large. Moreover, finite deformation is important in the analysis of some micro-scale phenomena where strain gradient effects are expected to be significant, such as plastic flow localization and crack tip fields.

The purpose of this paper is to develop a finite deformation theory of strain gradient plasticity. We begin with a review of the infinitesimal deformation theories in Section 2, including the phenomenological theory of strain gradient plasticity (Fleck and Hutchinson, 1997) and the mechanism-based strain gradient (MSG) plasticity theory derived from the Taylor (1938) dislocation model. We then generalize them to finite deformation theories in the reference configuration, and study the size effect in micro-indentation hardness experiments.

2. Review of strain gradient plasticity theories: infinitesimal deformation

The theories of strain gradient plasticity for infinitesimal deformation (Fleck and Hutchinson, 1997; Gao et al., 1999; Huang et al., 2000a, b) are summarized in this section.

2.1. Generalized stresses and strains

In a Cartesian reference frame x_i, the strain tensor ε_{ij} and strain gradient tensor η_{ijk} are related to the displacement u_i by

$$\varepsilon_{ij} = \tfrac{1}{2}(u_{i,j} + u_{j,i}) \tag{1}$$

and

$$\eta_{ijk} = u_{k,ij}, \tag{2}$$

which have the symmetry $\varepsilon_{ij} = \varepsilon_{ji}$ and $\eta_{ijk} = \eta_{jik}$. The strain gradient tensor can also be expressed directly in terms of the strain tensor, i.e.,

$$\eta_{ijk} = \varepsilon_{ik,j} + \varepsilon_{jk,i} - \varepsilon_{ij,k}. \tag{3}$$

The deviatoric strain and deviatoric strain gradient are defined as

$$\varepsilon'_{ij} = \varepsilon_{ij} - \tfrac{1}{3}\varepsilon_{kk}\delta_{ij}, \quad \eta'_{ijk} = \eta_{ijk} - \tfrac{1}{4}(\delta_{ik}\eta_{jpp} + \delta_{jk}\eta_{ipp}). \tag{4}$$

The virtual work per unit volume of the solid due to a variation of displacement δu_i is

$$\delta w = \sigma_{ij}\delta\varepsilon_{ij} + \tau_{ijk}\delta\eta_{ijk}, \tag{5}$$

where the symmetric Cauchy stress σ_{ij} is the work conjugate of the variation of strain $\delta\varepsilon_{ij}$, and the symmetric higher-order stress τ_{ijk} is the work conjugate of the variation of strain gradient $\delta\eta_{ijk}$.

2.2. Principle of virtual work: equilibrium equations and boundary conditions

The principle of virtual work gives (Fleck and Hutchinson, 1997)

$$\int_v (\sigma_{ij}\delta\varepsilon_{ij} + \tau_{ijk}\delta\eta_{ijk})\,\mathrm{d}v = \int_v f_k\delta u_k\,\mathrm{d}v + \int_a \left(t_k\delta u_k + r_k\frac{\partial\delta u_k}{\partial n}\right)\mathrm{d}a + \int_c p_k\delta u_k|\mathrm{d}\boldsymbol{x}|, \tag{6}$$

where f_k is the body force per unit volume, t_k and r_k are the stress traction and the higher order stress traction on the surface, n is the normal of the surface, and p_k is the line force (per unit length) on the edge c intercepted by two smooth surfaces.

The equilibrium equations can be obtained from the principle of virtual work,

$$\sigma_{ik,i} - \tau_{ijk,ij} + f_k = 0. \tag{7}$$

The stress tractions t_k and higher order stress tractions r_k on the surface of the body are

$$t_k = n_i(\sigma_{ik} - \tau_{ijk,j}) - D_j(n_i\tau_{ijk}) + n_i n_j\tau_{ijk}(D_q n_q), \tag{8}$$

$$r_k = n_i n_j\tau_{ijk}, \tag{9}$$

where n_i is the unit normal to the surface and D_j is the surface-gradient operator given by

$$D_j = (\delta_{jk} - n_j n_k)\frac{\partial}{\partial x_k}. \tag{10}$$

On the surface of the body, the gradient $\partial/\partial x_j$ can be decomposed to the above surface gradient D_j and a normal gradient $n_j D_n$, i.e.,

$$\frac{\partial}{\partial x_j} = D_j + n_j D_n, \tag{11}$$

where

$$D_n = n_k \frac{\partial}{\partial x_k}. \tag{12}$$

Only the deformation theory of strain gradient plasticity is presented in this paper. It is well known that a deformation theory mimics the effects of a corner on a yield surface, the latter being important in bifurcation phenomena. The flow theory of strain gradient plasticity can be established following the same approach.

2.3. Constitutive equations in the Fleck–Hutchinson strain gradient plasticity theory

The uniaxial stress–strain relation can be written as

$$\sigma = \sigma_{\text{ref}} f(\varepsilon), \tag{13}$$

where σ_{ref} is a reference stress in uniaxial tension and f is a function of strain. For most ductile materials, the function f can be written as a power law relation

$$f(\varepsilon) = \varepsilon^N, \tag{14}$$

where N is the plastic work hardening exponent ($0 \leqslant N < 1$).

The deformation theory of the Fleck–Hutchinson strain gradient plasticity theory (Fleck and Hutchinson, 1997) gives the stresses and higher-order stresses in terms of strain energy density w,

$$\sigma_{ij} = \frac{\partial w(\mathscr{E})}{\partial \varepsilon_{ij}}, \quad \tau_{ijk} = \frac{\partial w(\mathscr{E})}{\partial \eta_{ijk}}, \tag{15}$$

where w takes the form

$$w = \frac{1}{2}K\varepsilon_{kk}^2 + \sigma_{\text{ref}} \int_0^{\mathscr{E}} f(\mathscr{E})\,\mathrm{d}\mathscr{E} = \frac{1}{2}K\varepsilon_{kk}^2 + \frac{\sigma_{\text{ref}}}{N+1}\mathscr{E}^{N+1}, \tag{16}$$

K is the elastic bulk modulus, ε_{kk} is the volumetric strain, and $\mathscr{E}$ is a combined measure of effective strain and strain gradient, given by

$$\mathscr{E} = \sqrt{\tfrac{2}{3}\varepsilon'_{ij}\varepsilon'_{ij} + c_1\eta'_{iik}\eta'_{jjk} + c_2\eta'_{ijk}\eta'_{ijk} + c_3\eta'_{ijk}\eta'_{kji}}. \tag{17}$$

Here, c_1, c_2 and c_3 have the dimension of length squared, and are assumed to be material constants. From micro-torsion, micro-bending and micro-indentation experiments, Begley and Hutchinson (1998) have established

$$c_1 \approx 0, \quad c_2 \approx 0.17\,l^2, \quad c_3 \approx -0.16\,l^2, \tag{18}$$

where l is a material length parameter and is estimated to be 4 μm for copper and 6 μm for nickel. For plastic work hardening exponent $N = 1$, the Fleck–Hutchinson strain gradient plasticity theory degenerates to the linear elastic strain gradient theory (Toupin, 1962, 1964; Koiter, 1964; Mindlin, 1964, 1965).

2.4. Constitutive equations in the MSG plasticity theory

The flow stress in the mechanism-based strain gradient (MSG) plasticity theory (Gao et al., 1999; Huang et al., 2000a,b) is obtained from the Taylor dislocation model (1938) as

$$\sigma = \sigma_{\text{ref}} \sqrt{f^2(\varepsilon) + l\eta}, \tag{19}$$

where ε and η are the effective strain and effective strain gradient, respectively,

$$\varepsilon = \sqrt{\tfrac{2}{3}\varepsilon'_{ij}\varepsilon'_{ij}}, \quad \eta = \tfrac{1}{2}\sqrt{\eta'_{ijk}\eta'_{ijk}}. \tag{20}$$

The characteristic material length l in (19) associated with strain gradient plasticity is given in terms of shear modulus μ and Burgers vector b by (Huang et al., 1999)

$$l = 18\alpha^2 \left(\frac{\mu}{\sigma_{\text{ref}}}\right)^2 b, \tag{21}$$

where α is an empirical material constant between 0.1 and 0.5 in the Taylor dislocation model (1938). For metallic materials, the internal material length is indeed on the order of microns, consistent with the estimate by Fleck and Hutchinson (1997).

The constitutive equations in the deformation theory of MSG plasticity are

$$\sigma_{ij} = K\varepsilon_{kk}\delta_{ij} + \frac{2\sigma}{3\varepsilon}\varepsilon'_{ij}, \tag{22}$$

$$\tau_{ijk} = l_\varepsilon^2 \left[\frac{1}{6}K\eta^{\text{H}}_{ijk} + \frac{\sigma}{\varepsilon}(\Lambda_{ijk} - \Pi_{ijk}) + \frac{\sigma_{\text{ref}}^2 f(\varepsilon) f'(\varepsilon)}{\sigma}\Pi_{ijk}\right], \tag{23}$$

where the flow stress σ is given in (19), η^{H}_{ijk} is the volumetric part of the strain gradient tensor,

$$\eta^{\text{H}}_{ijk} = \tfrac{1}{4}(\delta_{ik}\eta_{jpp} + \delta_{jk}\eta_{ipp}), \tag{24}$$

and Λ_{ijk} and Π_{ijk} are given by

$$\Lambda_{ijk} = \frac{1}{72}\left[2\eta'_{ijk} + \eta'_{kij} + \eta'_{kji} + \frac{1}{2}\delta_{ij}\eta_{kpp} + \frac{1}{3}\eta^{\text{H}}_{ijk}\right], \tag{25}$$

$$\Pi_{ijk} = \frac{1}{54\varepsilon^2}\left[\varepsilon'_{mn}(\varepsilon'_{ik}\eta'_{jmn} + \varepsilon'_{jk}\eta'_{imn}) + \frac{1}{4}\eta_{qpp}(\varepsilon'_{ik}\varepsilon'_{jq} + \varepsilon'_{jk}\varepsilon'_{iq})\right]. \tag{26}$$

The length l_ε in Eq. (23) is the mesoscale cell size given by

$$l_\varepsilon = 10\frac{\mu}{\sigma_{\text{Y}}}b, \tag{27}$$

where σ_{Y} is the initial yield stress in uniaxial tension.

3. Strain gradient tensor

Let X_{I}, X_{II}, X_{III} be the Cartesian Lagrangian coordinates in the reference (initial) configuration $\mathscr{R}$, and x_1, x_2, x_3 the Eulerian coordinates in the current configuration r. The corresponding gradient operators in the reference and current configurations $\mathscr{R}$ and r are denoted by $\overset{<}{\nabla}$ and $\overset{>}{\nabla}$, respectively,

$$\varphi\overset{<}{\nabla} = \frac{\partial\varphi}{\partial X_A}\boldsymbol{e}_A, \quad \overset{<}{\nabla}\varphi = \boldsymbol{e}_A\frac{\partial\varphi}{\partial X_A},$$

$$\varphi\overset{>}{\nabla} = \frac{\partial\varphi}{\partial x_i}\boldsymbol{e}_i, \quad \overset{>}{\nabla}\varphi = \boldsymbol{e}_i\frac{\partial\varphi}{\partial x_i}, \tag{28}$$

where φ denotes any scalar or tensor fields, $\boldsymbol{e}_A$ $(A = \mathrm{I}, \mathrm{II}, \mathrm{III})$ and $\boldsymbol{e}_i$ $(i = 1, 2, 3)$ are unit vectors along coordinate axes X_A and x_i, respectively. The operators $\overset{<}{\nabla}$ and $\overset{>}{\nabla}$ are related by

$$\varphi\overset{<}{\nabla} = (\varphi\overset{>}{\nabla})\cdot\boldsymbol{F}, \quad \varphi\overset{>}{\nabla} = (\varphi\overset{<}{\nabla})\cdot\overset{-1}{\boldsymbol{F}},$$

$$\overset{<}{\nabla}\varphi = \boldsymbol{F}^{\mathrm{T}}\cdot(\overset{>}{\nabla}\varphi), \quad \overset{>}{\nabla}\varphi = \overset{-\mathrm{T}}{\boldsymbol{F}}\cdot(\overset{<}{\nabla}\varphi), \tag{29}$$

where $\boldsymbol{F}$ is deformation gradient, and $\overset{-1}{\boldsymbol{F}}, \boldsymbol{F}^{\mathrm{T}}, \overset{-\mathrm{T}}{\boldsymbol{F}}$ are its reciprocal, transpose, reciprocal transpose, respectively,

$$\boldsymbol{F} = \frac{\partial x_i}{\partial X_A}\boldsymbol{e}_i\boldsymbol{e}_A, \quad \boldsymbol{F}^{\mathrm{T}} = \frac{\partial x_i}{\partial X_A}\boldsymbol{e}_A\boldsymbol{e}_i,$$

$$\overset{-1}{\boldsymbol{F}} = \frac{\partial X_A}{\partial x_i}\boldsymbol{e}_A\boldsymbol{e}_i, \quad \overset{-\mathrm{T}}{\boldsymbol{F}} = \frac{\partial X_A}{\partial x_i}\boldsymbol{e}_i\boldsymbol{e}_A. \tag{30}$$

The Green strain tensor $\boldsymbol{E}$ is given in terms of the deformation gradient $\boldsymbol{F}$ by

$$\boldsymbol{E} = \tfrac{1}{2}(\boldsymbol{F}^{\mathrm{T}}\cdot\boldsymbol{F} - \mathbf{1}), \quad E_{AB} = \tfrac{1}{2}\left(\frac{\partial x_i}{\partial X_A}\frac{\partial x_i}{\partial X_B} - \delta_{AB}\right), \tag{31}$$

where $\mathbf{1}$ is second-order unit tensor and δ_{AB} is the Kronecker delta. For finite deformation, we define the strain gradient tensor in the reference configuration by replacing the infinitesimal strain ε_{ij} in Eq. (3) with the Green strain E_{IJ}, i.e.,

$$\eta_{IJK} = E_{IK,J} + E_{JK,I} - E_{IJ,K}. \tag{32}$$

It should be emphasized that the above strain gradient tensor is defined in the reference configuration and therefore meets the requirement of frame indifference.

4. Constitutive law of strain gradient plasticity

The finite-deformation constitutive relations are given for the Fleck–Hutchinson strain gradient plasticity (Fleck and Hutchinson, 1997) and MSG plasticity theories (Gao et al., 1999; Huang et al., 2000a,b) in the reference configuration. Therefore, the constitutive laws automatically meet the requirement of frame indifference.

4.1. Fleck–Hutchinson strain gradient plasticity theory

The combined measure $\mathscr{E}$ of effective strain and strain gradient in Eq. (17) can be generalized to finite deformation by replacing the infinitesimal strain and strain gradient with the Green strain and the finite strain gradient in Eq. (32), respectively, i.e.,

$$\mathscr{E} = \sqrt{\tfrac{2}{3}E'_{IJ}E'_{IJ} + c_1\eta'_{IIK}\eta'_{JJK} + c_2\eta'_{IJK}\eta'_{IJK} + c_3\eta'_{IJK}\eta'_{KJI}}, \tag{33}$$

where

$$E'_{IJ} = E_{IJ} - \tfrac{1}{3}E_{KK}\delta_{IJ}, \tag{34}$$

$$\eta'_{IJK} = \eta_{IJK} - \tfrac{1}{4}(\delta_{IK}\eta_{JPP} + \delta_{JK}\eta_{IPP}), \tag{35}$$

which are the generalizations of deviatoric strain and deviatoric strain gradient in Eq. (4). The constitutive equations in the deformation theory of strain gradient plasticity can be written as

$$\boldsymbol{T} = \frac{\partial w}{\partial \boldsymbol{E}}, \quad \boldsymbol{S} = \frac{\partial w}{\partial \boldsymbol{\eta}}, \tag{36}$$

where w is the strain energy per unit volume in the reference configuration $\mathscr{R}$, $\boldsymbol{T}$ is the second Piola–Kirchhoff stress tensor, and $\boldsymbol{S}$ is the higher-order stress tensor. A simple generalization of w from its infinitesimal deformation counterpart in Eq. (16) is

$$w(\boldsymbol{E}, \boldsymbol{\eta}) = \frac{1}{2}KE_{KK}^2 + \frac{\sigma_{\mathrm{ref}}}{N+1}\mathscr{E}^{N+1}. \tag{37}$$

It should also be pointed out that E_{KK} is not exactly the volumetric part of E_{IJ} in finite deformation. It only represents a simple generalization of ε_{kk} in the infinitesimal deformation. The substitution of Eq. (37) into Eq. (36) gives the second Piola–Kirchhoff stress as

$$\boldsymbol{T} = KE_{KK}\mathbf{1} + \frac{2\mathscr{J}}{3\mathscr{E}}\boldsymbol{E}', \tag{38}$$

where

$$\mathscr{J} = \frac{\partial w}{\partial \mathscr{E}} = \sigma_{\mathrm{ref}}\mathscr{E}^N, \tag{39}$$

and $\boldsymbol{E}'$ is given in Eq. (34). The higher-order stress $\boldsymbol{S}$ can also be obtained similarly.

4.2. MSG plasticity theory

The finite deformation theory of MSG plasticity can be straightforwardly obtained from Eqs. (22) and (23) by replacing the infinitesimal strain, strain gradient, stress and higher-order stress with the Green strain $\boldsymbol{E}$, strain gradient $\boldsymbol{\eta}$, second Piola–Kirchhoff stress $\boldsymbol{T}$, and higher-order stress $\boldsymbol{S}$, respectively, i.e.,

$$\begin{aligned} \boldsymbol{T} &= KE_{KK}\mathbf{1} + \frac{2T}{3E}\boldsymbol{E}', \\ \boldsymbol{S} &= l_\varepsilon^2\left[\frac{1}{6}K\boldsymbol{\eta}^{\mathrm{H}} + \frac{T}{E}(\boldsymbol{\Lambda} - \boldsymbol{\Pi}) + \frac{\sigma_{\mathrm{ref}}^2 f(E)f'(E)}{T}\boldsymbol{\Pi}\right], \end{aligned} \tag{40}$$

where $\boldsymbol{E}'$ is given in Eq. (34),

$$E = (\tfrac{2}{3}\boldsymbol{E}' : \boldsymbol{E}')^{1/2} = (\tfrac{2}{3}E'_{IJ}E'_{IJ})^{1/2} \tag{41}$$

is the generalization of the equivalent strain,

$$T = \sigma_{\text{ref}}\sqrt{f^2(E) + l\eta} \tag{42}$$

is the flow stress that has incorporated the effective strain gradient $\eta = \frac{1}{2}\sqrt{\eta'_{IJK}\eta'_{IJK}}$ with η'_{IJK} given in Eq. (35), $\boldsymbol{\eta}^{\text{H}}$ is the generalization of the volumetric part of strain gradient in Eq. (24),

$$\eta^{\text{H}}_{IJK} = \tfrac{1}{4}(\delta_{IK}\eta_{JPP} + \delta_{JK}\eta_{IPP}), \tag{43}$$

and $\boldsymbol{\Lambda}$ and $\boldsymbol{\Pi}$ are obtained from Eqs. (25) and (26) as

$$\Lambda_{IJK} = \frac{1}{72}\left[2\eta'_{IJK} + \eta'_{KJI} + \eta'_{KIJ} + \frac{1}{2}\delta_{IJ}\eta_{KPP} + \frac{1}{3}\eta^{\text{H}}_{IJK}\right], \tag{44}$$

$$\Pi_{IJK} = \frac{1}{54E^2}\left[E'_{MN}(E'_{IK}\eta'_{JMN} + E'_{JK}\eta'_{IMN}) + \frac{1}{4}\eta_{QPP}(E'_{IK}E'_{JQ} + E'_{JK}E'_{IQ})\right]. \tag{45}$$

5. Strain rate and strain gradient rate tensors

As shown in the next section, we need the strain rate and strain gradient rate tensors to derive the equilibrium equations in finite deformation from the principle of virtual work. The rate of deformation tensor $\boldsymbol{d}$ is defined as the symmetrization of velocity gradient $\boldsymbol{v}\overset{>}{\nabla}$,

$$\begin{aligned} \boldsymbol{d} &= \tfrac{1}{2}(\boldsymbol{v}\overset{>}{\nabla} + \overset{>}{\nabla}\boldsymbol{v}), \\ d_{ij} &= \tfrac{1}{2}(v_{i,j} + v_{j,i}). \end{aligned} \tag{46}$$

It is well known in continuum mechanics that $\boldsymbol{d}$ (or $\dot{\boldsymbol{E}}$) is the covariant push-forward (or pull-back) of the rate of Green strain $\dot{\boldsymbol{E}}$ (or $\boldsymbol{d}$),

$$\begin{aligned} &\boldsymbol{d} = \overset{-\text{T}}{\boldsymbol{F}} \cdot \dot{\boldsymbol{E}} \cdot \overset{-1}{\boldsymbol{F}} = (\overset{-\text{T}-\text{T}}{\boldsymbol{F}\ \boldsymbol{F}}) * * \dot{\boldsymbol{E}}, \quad d_{ij} = \frac{\partial X_A}{\partial x_i}\frac{\partial X_B}{\partial x_j}\dot{E}_{AB}, \\ &\dot{\boldsymbol{E}} = \boldsymbol{F}^{\text{T}} \cdot \boldsymbol{d} \cdot \boldsymbol{F} = (\boldsymbol{F}^{\text{T}}\boldsymbol{F}^{\text{T}}) * * \boldsymbol{d}, \quad \dot{E}_{AB} = \frac{\partial x_i}{\partial X_A}\frac{\partial x_j}{\partial X_B}d_{ij}. \end{aligned} \tag{47}$$

Here the symbol "**" denotes the scalar product by each of the entities before the symbol with each corresponding [1] vector of the dyadic after the symbol. For example, if $\boldsymbol{A}$ and $\boldsymbol{B}$ are tensors, operating $\boldsymbol{AB}$ on a dyadic $\boldsymbol{ab}$ is defined by

$$(\boldsymbol{AB}) * *(\boldsymbol{ab}) = (\boldsymbol{A} \cdot \boldsymbol{a})(\boldsymbol{B} \cdot \boldsymbol{b}). \tag{48}$$

[1] The correspondence is understood to follow the order of appearance from Left to Right.

The gradient of the rate of Green strain is obtained by differentiating Eq. (47) with respect to coordinate X_C,

$$\dot{E}_{AB,C} = \left(\frac{\partial x_i}{\partial X_A}\frac{\partial x_j}{\partial X_B}d_{ij}\right)_{,C} = \frac{\partial x_i}{\partial X_A}\frac{\partial x_j}{\partial X_B}\frac{\partial x_k}{\partial X_C}d_{ij,k} + \left(\frac{\partial x_i}{\partial X_A}\frac{\partial x_j}{\partial X_B}\right)_{,C} d_{ij},$$

$$\dot{\boldsymbol{E}}\overset{<}{\nabla} = (\boldsymbol{F}^{\mathrm{T}}\boldsymbol{F}^{\mathrm{T}}\boldsymbol{F}^{\mathrm{T}}) * * * (\boldsymbol{d}\overset{>}{\nabla}) + [(\boldsymbol{F}^{\mathrm{T}}\boldsymbol{F}^{\mathrm{T}})\overset{<}{\nabla}] * * \boldsymbol{d}. \tag{49}$$

Here the first term on the right-hand side is the covariant pull-back of $\boldsymbol{d}\overset{>}{\nabla}$, and the symbol "$***$" is understood in a sense similar to "$**$" in Eq. (48).

The second Piola–Kirchhoff stress $\boldsymbol{T}$ and higher-order stress $\boldsymbol{S}$ are the work conjugates of $\boldsymbol{E}$ and $\boldsymbol{\eta}$, respectively. The rate of work can be expressed as

$$\dot{w} = \boldsymbol{T} : \dot{\boldsymbol{E}} + \boldsymbol{S}\dddot{:}\dot{\boldsymbol{\eta}} = T_{AB}\dot{E}_{AB} + S_{ABC}\dot{\eta}_{ABC}, \tag{50}$$

where $\dddot{:}$ is the symbol of triple dot, and $\dot{\eta}_{ABC}$ is related to the gradient of rate of Green tensor $\dot{E}_{AB,C}$ via Eq. (32) by

$$\dot{\eta}_{ABC} = \dot{E}_{CA,B} + \dot{E}_{CB,A} - \dot{E}_{AB,C}. \tag{51}$$

For the principle of virtual work used in the next section, it is useful to express the rate of work $\dot{w}$ in terms of the Cauchy stress $\boldsymbol{\sigma}$ and the rate of deformation $\boldsymbol{d}$ in the current configuration r. Let J be the volume ratio, i.e., the determinant of $\boldsymbol{F}$,

$$J = \det\left|\frac{\partial x_i}{\partial X_A}\right|. \tag{52}$$

The Kirchhoff stress $J\boldsymbol{\sigma}$ and second Piola–Kirchhoff stress $\boldsymbol{T}$ are related by contravariant push-forward or pull-back operation

$$J\boldsymbol{\sigma} = (\boldsymbol{F}\boldsymbol{F}) * * \boldsymbol{T}, \quad J\sigma_{ij} = \frac{\partial x_i}{\partial X_A}\frac{\partial x_j}{\partial X_B}T_{AB},$$

$$\boldsymbol{T} = (\boldsymbol{F}^{-1}\boldsymbol{F}^{-1}) * * J\boldsymbol{\sigma}, \quad T_{AB} = \frac{\partial X_A}{\partial x_i}\frac{\partial X_B}{\partial x_j}J\sigma_{ij}. \tag{53}$$

In a similar manner, we define the higher-order stress $\boldsymbol{\tau}$ in the current configuration r as the contravariant push-forward of $\boldsymbol{S}$ from the reference configuration $\mathscr{R}$ to the current configuration r,

$$J\boldsymbol{\tau} = (\boldsymbol{F}\boldsymbol{F}\boldsymbol{F}) * * * \boldsymbol{S}, \quad J\tau_{ijk} = \frac{\partial x_i}{\partial X_A}\frac{\partial x_j}{\partial X_B}\frac{\partial x_k}{\partial X_C}S_{ABC},$$

$$\boldsymbol{S} = (\overset{-1-1-1}{\boldsymbol{F}\ \boldsymbol{F}\ \boldsymbol{F}}) * * * J\boldsymbol{\tau}, \quad S_{ABC} = \frac{\partial X_A}{\partial x_i}\frac{\partial X_B}{\partial x_j}\frac{\partial X_C}{\partial x_k}J\tau_{ijk}. \tag{54}$$

Making use of the relations for stresses and strain rates between the reference and current configurations, the rate of work $\dot{w}$ can be written as

$$\dot{w} = J\tilde{\boldsymbol{\sigma}} : \boldsymbol{d} + J\boldsymbol{\tau}\dddot{:}\boldsymbol{\zeta} = J\tilde{\sigma}_{ij}d_{ij} + J\tau_{ijk}\zeta_{ijk}, \tag{55}$$

where $\boldsymbol{\zeta}$ is the strain rate gradient tensor in the current configuration,

$$\boldsymbol{\zeta} = \boldsymbol{v}\overset{>}{\nabla}\overset{>}{\nabla}, \quad \zeta_{ijk} = v_{k,ij}, \tag{56}$$

$\tilde{\boldsymbol{\sigma}}$ is the modified Cauchy stress that combines the Cauchy stress $\boldsymbol{\sigma}$ and the higher order stress,

$$J\tilde{\boldsymbol{\sigma}} \triangleq J\boldsymbol{\sigma} + \boldsymbol{s}^*,$$

$$J\tilde{\sigma}_{ij} \triangleq J\sigma_{ij} + s^*_{ij}, \tag{57}$$

and $\boldsymbol{s}^*$ is given by

$$s^*_{ij} = \left(\frac{\partial x_i}{\partial X_A}\frac{\partial x_j}{\partial X_B}\right)_{,C}(S_{CAB} + S_{CBA} - S_{ABC}). \tag{58}$$

It is observed that $\tilde{\boldsymbol{\sigma}}$ is similar to the equivalent transverse shear force in Kirchhoff's thin plate theory, which is a combination of transverse shear force and the gradient of the twisting moment.

6. Principle of virtual work: equilibrium equations and boundary conditions

The equilibrium equations and boundary conditions are established from the principle of virtual work in this section. The solid, which occupies the region $\mathscr{V}$ in the reference configuration $\mathscr{R}$, deforms to the region v in the current configuration r. Similarly, the surface $\mathscr{A}$ deforms to a, and the edge $\mathscr{C}$ (if present) formed by the intersection of two smooth surface segments $\mathscr{A}^{(1)}$ and $\mathscr{A}^{(2)}$ deforms to the edge c formed by the corresponding deformed surface segments $a^{(1)}$ and $a^{(2)}$. Let $\mathscr{N}$ and $\boldsymbol{n}$ be the unit normal vectors of $\mathscr{A}$ and a, and $\mathscr{C}$ and $\boldsymbol{c}$ be the unit vectors tangential to $\mathscr{C}$ and c, and $\mathscr{K}^{(1)}, \mathscr{K}^{(2)}, \boldsymbol{k}^{(1)}$ and $\boldsymbol{k}^{(2)}$ be the unit normals to $\mathscr{C}$ and c, lying within $\mathscr{A}^{(1)}, \mathscr{A}^{(2)}, a^{(1)}$ and $a^{(2)}$, respectively,

$$\mathscr{K}^{(1)} = \mathscr{C}^{(1)} \times \mathscr{N}^{(1)}, \quad \mathscr{K}^{(2)} = \mathscr{C}^{(2)} \times \mathscr{N}^{(2)},$$

$$\boldsymbol{k}^{(1)} = \boldsymbol{c}^{(1)} \times \boldsymbol{n}^{(1)}, \quad \boldsymbol{k}^{(2)} = \boldsymbol{c}^{(2)} \times \boldsymbol{n}^{(2)}. \tag{59}$$

The principle of virtual work in the current configuration can be established from its counterpart in Eq. (6) for infinitesimal strain by replacing the virtual displacement $\delta\boldsymbol{u}$ with virtual velocity $\boldsymbol{v}$, and replacing the stress $\boldsymbol{\sigma}$ with the modified Cauchy stress $\tilde{\boldsymbol{\sigma}}$ according to Eqs. (50) and (55),

$$\int_v [\tilde{\boldsymbol{\sigma}} : \boldsymbol{d} + \boldsymbol{\tau} \vdots \boldsymbol{\zeta}]\,\mathrm{d}v = \int_v (\boldsymbol{f}\cdot\boldsymbol{v})\,\mathrm{d}v + \int_a (\boldsymbol{t}\cdot\boldsymbol{v})\,\mathrm{d}a + \int_a \boldsymbol{r}\cdot\frac{\partial \boldsymbol{v}}{\partial n}\,\mathrm{d}a + \sum_n \oint_{c_n} \boldsymbol{p}\cdot\boldsymbol{v}|\,\mathrm{d}\boldsymbol{x}|, \tag{60}$$

where the virtual rate of deformation $\boldsymbol{d}$ and its gradient $\boldsymbol{\zeta}$ are related to the virtual velocity $\boldsymbol{v}$ via Eqs. (46) and (56), respectively, $\boldsymbol{f}$ is the body force per unit volume in current configuration r, $\boldsymbol{t}$ and $\boldsymbol{r}$ are the stress traction and the higher stress traction per unit area on the surface a, respectively, and $\boldsymbol{p}$ is line load per unit length of the edge c. Based on Eq. (60) and the divergence theorem, the equilibrium equations and traction boundary conditions in the current configuration r can be established as

$$\overset{>}{\nabla}\cdot(\tilde{\boldsymbol{\sigma}} - \overset{>}{\nabla}\cdot\boldsymbol{\tau}) + \boldsymbol{f} = \boldsymbol{0} \quad \text{in } v,$$

$$\partial_i[\tilde{\sigma}_{ik} - \partial_j(\tau_{ijk})] + f_k = 0, \tag{61}$$

$$\boldsymbol{n}\cdot(\tilde{\boldsymbol{\sigma}}-\overset{>}{\nabla}\cdot\boldsymbol{\tau})+(\boldsymbol{nn}:\boldsymbol{\tau})(\overset{>}{\boldsymbol{D}}\cdot\boldsymbol{n})-\overset{>}{\boldsymbol{D}}\cdot(\boldsymbol{n}\cdot\boldsymbol{\tau})=\boldsymbol{t}\quad\text{on } a,$$

$$n_i(\tilde{\sigma}_{ik}-\partial_j\tau_{ijk})+n_in_j\tau_{ijk}(D_pn_p)-D_j(n_i\tau_{ijk})=t_k, \tag{62}$$

$$\boldsymbol{nn}:\boldsymbol{\tau}=\boldsymbol{r}\quad\text{on } a,$$

$$n_in_j\tau_{ijk}=r_k, \tag{63}$$

$$\boldsymbol{n}^{(1)}\cdot(\boldsymbol{k}^{(1)}\cdot\boldsymbol{\tau})+\boldsymbol{n}^{(2)}\cdot(\boldsymbol{k}^{(2)}\cdot\boldsymbol{\tau})=(\boldsymbol{n}^{(1)}\boldsymbol{k}^{(1)}+\boldsymbol{n}^{(2)}\boldsymbol{k}^{(2)}):\boldsymbol{\tau}=\boldsymbol{p}\quad\text{on } c,$$

$$n_i^{(1)}k_j^{(1)}\tau_{ijk}+n_i^{(2)}k_j^{(2)}\tau_{ijk}=p_k, \tag{64}$$

where $\partial_i=\partial/\partial x_i$ is the gradient in the current configuration, $\overset{>}{\boldsymbol{D}}$ is the gradient operator on the surface a,

$$\overset{>}{\boldsymbol{D}}(\ldots)=\overset{>}{\nabla}(\ldots)-\boldsymbol{n}n\cdot\overset{>}{\nabla}(\ldots). \tag{65}$$

Since the kinematic relations and the constitutive law are given in the reference configuration $\mathscr{R}$, it is convenient to rewrite the equilibrium equations (61) and boundary conditions (62)–(64) in terms of the second Piola–Kirchhoff stress $\boldsymbol{T}$, higher-order stress $\boldsymbol{S}$, and gradient operator $\overset{<}{\nabla}$ in the reference configuration $\mathscr{R}$. With Eqs. (50) and (55), the left-hand side of Eq. (60) can be written as

$$\int_{\mathscr{V}}[\boldsymbol{T}:\dot{\boldsymbol{E}}+\boldsymbol{S}\vdots\dot{\boldsymbol{\eta}}]\,\mathrm{d}\mathscr{V}, \tag{66}$$

where the integration is over the region $\mathscr{V}$ in the reference configuration. The right-hand side of Eq. (60) can also be transformed to give the principle of virtual work in the reference configuration as

$$\int_{\mathscr{V}}(\boldsymbol{T}:\delta\boldsymbol{E}+\boldsymbol{S}\vdots\delta\boldsymbol{\eta})\,\mathrm{d}\mathscr{V}=\int_{\mathscr{V}}(J\boldsymbol{f})\cdot\delta\boldsymbol{u}\,\mathrm{d}\mathscr{V}+\int_{\mathscr{A}}(a_N\boldsymbol{t})\cdot\delta\boldsymbol{u}\,\mathrm{d}\mathscr{A}$$
$$+\int_{\mathscr{A}}(a_N\boldsymbol{r})\cdot\frac{\partial\delta\boldsymbol{u}}{\partial n}\,\mathrm{d}\mathscr{A}+\sum_n\oint_{\mathscr{C}_n}(\varepsilon_{\mathscr{C}}\boldsymbol{p})\cdot\delta\boldsymbol{u}|\,\mathrm{d}\boldsymbol{X}|, \tag{67}$$

where $\delta\boldsymbol{u}$ is the virtual displacement, $\delta\boldsymbol{E}$ and $\delta\boldsymbol{\eta}$ are the corresponding virtual variations of the Green strain $\boldsymbol{E}$ and strain gradient $\boldsymbol{\eta}$, a_N is the area ratio on $\mathscr{A}$, and ε_C is the length ratio on $\mathscr{C}$, which are discussed in the following.

The well-known Nanson's formula

$$\mathrm{d}\boldsymbol{a}=J\overset{-1}{\boldsymbol{F}}\cdot\mathrm{d}\boldsymbol{A} \tag{68}$$

has been used in the transformation of area element $\mathrm{d}\boldsymbol{A}$ in $\mathscr{R}$ to $\mathrm{d}\boldsymbol{a}$ in r, where $\mathrm{d}\boldsymbol{a}=|\mathrm{d}\boldsymbol{a}|\boldsymbol{n}$, $\mathrm{d}\boldsymbol{A}=|\mathrm{d}\boldsymbol{A}|\boldsymbol{N}$. The area ratio $a_N=|\mathrm{d}\boldsymbol{a}|/|\mathrm{d}\boldsymbol{A}|$ can be obtained straightforwardly from Eq. (68) as

$$a_N=J(\boldsymbol{N}\cdot\overset{-1}{\boldsymbol{F}}\cdot\overset{-\mathrm{T}}{\boldsymbol{F}}\cdot\boldsymbol{N})^{1/2}. \tag{69}$$

Similarly, the length ratio $\varepsilon_{\mathscr{C}} = |\mathrm{d}\boldsymbol{x}|/|\mathrm{d}\boldsymbol{X}|$ can be obtained from $\mathrm{d}\boldsymbol{x} = \boldsymbol{F}\cdot\mathrm{d}\boldsymbol{X}$ as

$$\varepsilon_{\mathscr{C}} = (\mathscr{C}\cdot\boldsymbol{F}^{\mathrm{T}}\cdot\boldsymbol{F}\cdot\mathscr{C})^{1/2}, \tag{70}$$

where $\mathscr{C}$ is the unit vector tangential to the edge $\mathscr{C}$.

The modified second Piola–Kirchhoff stress, $\tilde{\boldsymbol{T}}$, is defined as the contravariant pull-back of the modified Cauchy stress $\tilde{\boldsymbol{\sigma}}$, i.e.,

$$J\tilde{\boldsymbol{\sigma}} = (\boldsymbol{F}\boldsymbol{F}) ** \tilde{\boldsymbol{T}}, \quad J\tilde{\sigma}_{ij} = \frac{\partial x_i}{\partial X_A}\frac{\partial x_j}{\partial X_B}\tilde{T}_{AB},$$

$$\tilde{\boldsymbol{T}} = (\overset{-1}{\boldsymbol{F}}\,\overset{-1}{\boldsymbol{F}}) ** J\tilde{\boldsymbol{\sigma}}, \quad \tilde{T}_{AB} = \frac{\partial X_A}{\partial x_i}\frac{\partial X_B}{\partial x_j}J\tilde{\sigma}_{ij}. \tag{71}$$

The detailed derivations of the equilibrium equations and boundary conditions in the reference configurations are given in the appendix. The equilibrium equations (61) can be expressed in the reference configuration $\mathscr{R}$ as

$$\overset{<}{\nabla}\cdot\langle\tilde{\boldsymbol{T}}\cdot\boldsymbol{F}^{\mathrm{T}} - \overset{-1}{\boldsymbol{F}}\cdot\{\overset{<}{\nabla}\cdot[(\mathbf{1}\boldsymbol{F}\boldsymbol{F}) *** \boldsymbol{S}]\}\rangle + J\boldsymbol{f} = \boldsymbol{0},$$

$$\frac{\mathrm{d}}{\mathrm{d}X_A}\left[\tilde{T}_{AB}\frac{\partial x_i}{\partial X_B} - \frac{\partial X_A}{\partial x_j}\frac{\partial}{\partial X_B}\left(\delta_{BL}\frac{\partial x_j}{\partial X_M}\frac{\partial x_i}{\partial X_N}S_{LMN}\right)\right] + Jf_i = 0, \tag{72}$$

where $\mathrm{d}/\mathrm{d}X_A$ denotes "total partial derivative" with respect to X_A,

$$\frac{\mathrm{d}}{\mathrm{d}X_A} = \frac{\partial}{\partial X_A} + \frac{\partial x_k}{\partial X_A}\frac{\partial}{\partial x_k}. \tag{73}$$

The stress traction boundary condition (62) becomes

$$\boldsymbol{N}\cdot\tilde{\boldsymbol{T}}\cdot\boldsymbol{F}^{\mathrm{T}} - \boldsymbol{N}\cdot\overset{-1}{\boldsymbol{F}}\cdot\overset{<}{\nabla}\cdot[(\mathbf{1}\boldsymbol{F}\boldsymbol{F}) *** \boldsymbol{S}] - \overset{<}{\nabla}_S\cdot\boldsymbol{B}_T = a_N\boldsymbol{t} \quad \text{on } a,$$

$$N_A\tilde{T}_{AB}\frac{\partial x_i}{\partial X_B} - N_A\frac{\partial X_A}{\partial x_j}\frac{\partial}{\partial X_B}\left(\delta_{BL}\frac{\partial x_j}{\partial X_M}\frac{\partial x_i}{\partial X_N}S_{LMN}\right) - (\overset{<}{\nabla}_S\cdot B_T)_i = a_n t_i, \tag{74}$$

where $\overset{<}{\nabla}_S$ is the gradient operator on the surface $\mathscr{A}$, $\boldsymbol{B}_T$ is a second-order tensor given by

$$\boldsymbol{B}_T = (\boldsymbol{B}_T)_{Cl}\boldsymbol{e}_C\boldsymbol{e}_l,$$

$$(\boldsymbol{B}_T)_{Cl} = \frac{J}{a_N}e_{ijk}e_{ABC}\frac{\partial x_j}{\partial X_A}\frac{\partial X_M}{\partial x_k}N_M N_B(b_t)_{il}. \tag{75}$$

Here the tensor $\boldsymbol{b}_t$ is defined by

$$\boldsymbol{b}_t = \frac{1}{a_N}[(\boldsymbol{N}\boldsymbol{F}\boldsymbol{F}) *** \boldsymbol{S} - J\overset{-\mathrm{T}}{\boldsymbol{F}}\cdot\boldsymbol{N}\boldsymbol{r}] = (\boldsymbol{b}_t)_{il}\boldsymbol{e}_i\boldsymbol{e}_l, \tag{76}$$

and $\boldsymbol{r}$ is the higher-order stress traction as in Eq. (63).

In terms of the Gaussian coordinates $\Xi_{\mathrm{I}}, \Xi_{\mathrm{II}}$ along the principal curvature directions $\boldsymbol{i}_{(\mathrm{I})}$ and $\boldsymbol{i}_{(\mathrm{II})}$ on surface $\mathscr{A}$, $\overset{<}{\nabla}_S\cdot\boldsymbol{B}_T$ in Eq. (74) can be expressed as

$$\begin{aligned}\overset{<}{\nabla}_S\cdot\boldsymbol{B}_T &= \frac{1}{A_{(\mathrm{I})}}\frac{\partial\boldsymbol{B}_{T(\mathrm{I})}}{\partial\Xi_{\mathrm{I}}} + \frac{1}{A_{(\mathrm{II})}}\frac{\partial\boldsymbol{B}_{T(\mathrm{II})}}{\partial\Xi_{\mathrm{II}}} + \frac{1}{A_{(I)}A_{(\mathrm{II})}}\left(\frac{\partial A_{(\mathrm{II})}}{\partial\Xi_1}\boldsymbol{B}_{T(\mathrm{I})} + \frac{\partial A_{(\mathrm{I})}}{\partial\Xi_{\mathrm{II}}}\boldsymbol{B}_{T(\mathrm{II})}\right)\\ &= (\overset{<}{\nabla}_S\cdot\boldsymbol{B}_T)_i\boldsymbol{e}_i,\end{aligned} \tag{77}$$

where $A_{(\mathrm{I})}$ and $A_{(\mathrm{II})}$ are the corresponding Lamé parameters, and

$$\boldsymbol{B}_{T(\mathrm{I})} = \boldsymbol{i}_{(\mathrm{I})} \cdot \boldsymbol{B}_T, \quad \boldsymbol{B}_{T(\mathrm{II})} = \boldsymbol{i}_{(\mathrm{II})} \cdot \boldsymbol{B}_T.$$

The higher-order stress traction boundary condition (63) can be straightforwardly expressed as

$$J(\boldsymbol{NNF}) * * * \boldsymbol{S} = a_N \boldsymbol{r},$$

$$JN_A N_B \frac{\partial x_i}{\partial X_C} S_{ABC} = a_N r_i. \tag{78}$$

Similarly, the line traction boundary condition (64) on the edge $\mathscr{C}$ is given by

$$\varepsilon_{\mathscr{C}}(\boldsymbol{n}^{(1)}\boldsymbol{k}^{(1)} + \boldsymbol{n}^{(2)}\boldsymbol{k}^{(2)}) : [(\boldsymbol{FFF}) * * * \boldsymbol{S}] = \varepsilon_{\mathscr{C}} \boldsymbol{p},$$

$$\frac{\varepsilon_{\mathscr{C}}}{J}(n_i^{(1)}k_j^{(1)} + n_i^{(2)}k_j^{(2)}) \frac{\partial x_i}{\partial X_A} \frac{\partial x_j}{\partial X_B} \frac{\partial x_l}{\partial X_C} S_{ABC} = \varepsilon_{\mathscr{C}}\, p_l, \tag{79}$$

where $\boldsymbol{n} = J/a_N \overset{-\mathrm{T}}{\boldsymbol{F}} \cdot \boldsymbol{N}$ is the unit normal of the deformed surface, $\boldsymbol{k} = \boldsymbol{c} \times \boldsymbol{n}$, and $\boldsymbol{c} = (1/\varepsilon_{\mathscr{C}})\boldsymbol{F} \cdot \boldsymbol{C}$ is the unit vector along the deformed edge.

7. Finite deformation modeling of the micro-indentation experiment

Micro-indentation is a widely used experimental method to probe mechanical properties of materials at micron or sub-micron scales. These experiments have repeatedly shown that the indentation hardness depends strongly on the depth of indentation, the smaller the harder. Such size effect has been attributed to strain gradient hardening associated with the geometrically necessary dislocations. Accordingly, the theories of strain gradient plasticity (Fleck and Hutchinson, 1993, 1997; Gao et al., 1999; Huang et al., 2000a, b) have been developed to capture the size effects in micro-indentation. Begley and Hutchinson (1998) and Shu and Fleck (1998) have used the micro-indentation hardness data to determine the intrinsic material lengths in Eq. (18) for the Fleck–Hutchinson theory (Fleck et al., 1994; Fleck and Hutchinson, 1997). Huang et al. (2000b) and Qiu et al. (2001) have used the deformation and flow theories of MSG plasticity to model the micro-indentation experiment. With the Taylor coefficient $\alpha = 0.30$, they have found that the indentation hardness predicted by MSG plasticity theory agrees very well with McElhaney et al.'s (1998) hardness data for a wide range of indentation depth, ranging from 0.1 μm to several microns. It is encouraging that the Taylor coefficient $\alpha = 0.30$ has the correct order of magnitude (from 0.1 to 0.5).

The strain gradient theories used in the previous studies of micro-indentation are all limited to infinitesimal strains. It is anticipated that strains near the indenter tip can be relatively large, and it is therefore important to assess the effect of finite deformation in micro-indentation experiments. In the following, we use the finite deformation theory of MSG plasticity developed in this paper to investigate this issue. This will not only provide an estimate of finite deformation effects in micro-indentation, but also an important validation of the proposed finite deformation theory.

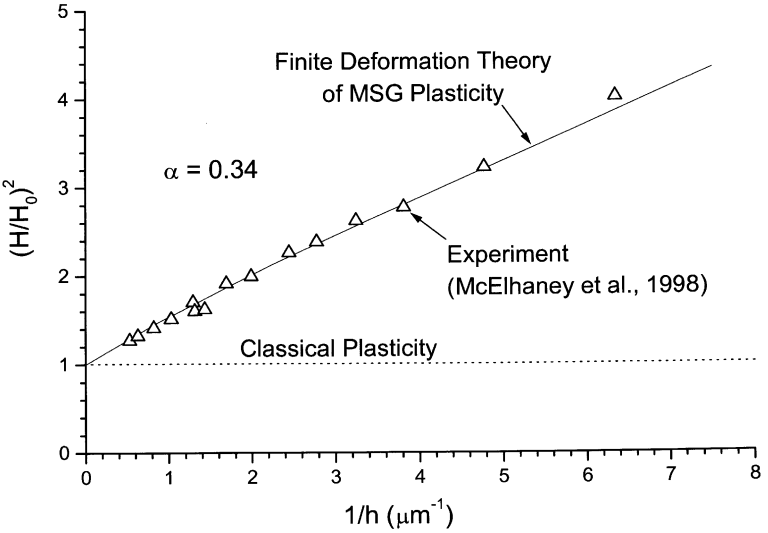

Fig. 1. Depth dependence of the hardness for polycrystalline copper. The solid line is the predicted hardness based on the finite deformation theory of MSG plasticity. The triangles are experimental data of McElhaney et al. (1998). H is the micro-indentation hardness, h is the depth of indentation, and $H_0 = 834$ MPa is the indentation hardness for a large indentation depth. Other material properties are shear modulus $\mu = 42$ GPa, Poisson's ratio $\nu = 0.3$, Burgers vector $b = 0.255$ nm, uniaxial stress–strain relation $\sigma = 441\varepsilon^{0.3}$ MPa, and Taylor coefficient $\alpha = 0.34$.

A finite element method is established for the finite deformation theory of MSG plasticity from the principle of virtual work, (Eq. (67)). Different elements for strain gradient plasticity have been used to check the accuracy of the numerical method, including the triangular C_1 element (Xia and Hutchinson, 1996; Begley and Hutchinson, 1998; Huang et al., 2000b), the hybrid element (Xia and Hutchinson, 1996; Shu and Fleck, 1998; Shu et al., 1999; Huang et al., 2000b), and the higher-order isoparametric element (Wei and Hutchinson, 1997; Huang et al., 2000b; Jiang et al., 2001). These elements have been shown to give consistent numerical results.

We have also adopted the same indentation model as in the previous studies of Begley and Hutchinson (1998), Shu and Fleck (1998), and Huang et al. (2000b). The effect of indenter pile-up (or sink-in) as well as the effect of the indenter tip radius have been accounted for in this model. Following Begley and Hutchinson (1998) and Huang et al. (2000b), the indenter is assumed to be axisymmetric with the half-angle of 72°, simulating a Vickers indenter.

Fig. 1 shows the micro-indentation hardness predicted by the finite deformation MSG theory for polycrystalline copper. The square of the indentation hardness, $(H/H_0)^2$, is plotted against the inverse of indentation depth, $1/h$, as suggested by Nix and Gao (1998), where H is the micro-indentation hardness and H_0 is the indentation hardness for large depth of indentation (i.e., without strain gradient effects). The shear modulus of copper is taken to be $\mu = 42$ GPa, Poisson ratio $\nu = 0.3$ (McElhaney

et al., 1998), Burgers vector $b=0.255$ nm, and Taylor coefficient $\alpha=0.34$. The uniaxial stress–strain law after plastic yielding can be written as a power law, $\sigma=441\varepsilon^{0.3}$ MPa, where the work hardening exponent 0.3 is consistent with that reported by McLean (1962) and Fleck et al. (1994) for polycrystalline copper. Based on this uniaxial stress–strain law, the finite element method predicts an indentation hardness $H_0 = 834$ MPa at a large indentation depth (without strain gradient effects), which agrees with the measured value of H_0 (McElhaney et al., 1998). The experimental hardness data of McElhaney et al. (1998) are shown in Fig. 1 for comparison. It is clearly observed that the numerically predicted hardness based on the finite deformation theory of MSG plasticity agrees very well with the experimental data over a wide range of indentation depth, from one-tenth of a micron to several microns. The Taylor coefficient $\alpha = 0.34$ in Fig. 1 for the finite deformation theory of MSG plasticity is slightly larger than its counterpart $\alpha = 0.30$ for the infinitesimal deformation theory of MSG plasticity (Huang et al., 2000b; Qiu et al., 2001), although both give very good agreement with the experimental hardness data and both have the right order of magnitude (between 0.1 and 0.5). Therefore, finite deformation does have some effect in micro-indentation experiments, as reflected from the relatively small change (0.34 versus 0.30) in the Taylor coefficient α. This change is not very significant since the Taylor coefficient is expected to have some uncertainties in that range.

8. Summary

We have developed the finite deformation theories of strain gradient plasticity by generalizing the infinitesimal deformation theories of Fleck and Hutchinson (1997), Gao et al. (1999) and Huang et al. (2000a, b). All kinematic relations and the constitutive laws are given in the reference configuration, and therefore meet the requirement of frame indifference. Based on the principle of virtual work, the equilibrium equations and traction boundary conditions are established in the current configuration and then transformed back to the reference configuration. The finite deformation theory of mechanism-based strain gradient (MSG) plasticity is used to study micro-indentation experiments. We show that the indentation hardness predicted by the finite deformation theory of MSG plasticity agrees very well with the experimental data. It is observed that finite deformation does have some effect in micro-indentation, although this effect is not very significant.

Acknowledgements

KCH acknowledges the support from the Ministry of Education, China. YH acknowledges NSF (grant CMS-0084980 and a supplement to grant CMS-9896285 from NSF International Program). HG acknowledges NSF (grant CMS-9979717). The support from NSFC is also acknowledged.

Appendix

Based on the divergence theorem and Nanson's formula (68), it is straightforward to show

$$J(\overset{>}{\nabla}\boldsymbol{\pi}) = \overset{<}{\nabla}\cdot(J\overset{-1}{\boldsymbol{F}}\boldsymbol{\pi}), \qquad J(\boldsymbol{\pi}\overset{>}{\nabla}) = (J\boldsymbol{\pi}\overset{-\mathrm{T}}{\boldsymbol{F}})\cdot\overset{<}{\nabla},$$

$$J(\overset{>}{\nabla}\cdot\boldsymbol{\pi}) = \overset{<}{\nabla}\cdot(J\overset{-1}{\boldsymbol{F}}\cdot\boldsymbol{\pi}), \qquad J(\boldsymbol{\pi}\cdot\overset{>}{\nabla}) = (J\boldsymbol{\pi}\cdot\overset{-\mathrm{T}}{\boldsymbol{F}})\cdot\overset{<}{\nabla}, \tag{A.1}$$

where $\boldsymbol{\pi}$ is a tensor of any rank. The equilibrium equations (61) can be rewritten via Eq. (80) to give

$$\boldsymbol{f} = -\overset{>}{\nabla}\cdot(\tilde{\boldsymbol{\sigma}} - \overset{>}{\nabla}\cdot\boldsymbol{\tau}) = -\frac{1}{J}\overset{<}{\nabla}\cdot\left\{J\overset{-1}{\boldsymbol{F}}\cdot\tilde{\boldsymbol{\sigma}} - J\overset{-1}{\boldsymbol{F}}\cdot\left[\frac{1}{J}\overset{<}{\nabla}\cdot(J\overset{-1}{\boldsymbol{F}}\cdot\boldsymbol{\tau})\right]\right\}.$$

Further use of Eqs. (54) and (71) leads to

$$\boldsymbol{f} = -\frac{1}{J}\overset{<}{\nabla}\cdot\langle\tilde{\boldsymbol{T}}\cdot\boldsymbol{F}^{\mathrm{T}} - \overset{-1}{\boldsymbol{F}}\cdot\{\overset{<}{\nabla}\cdot[(\mathbf{1}\boldsymbol{F}\boldsymbol{F})***\boldsymbol{S}]\}\rangle,$$

which is the same as the equilibrium equation (72).

In order to transform the traction boundary condition (62) from the current configuration r to the reference configuration $\mathscr{R}$, we need to establish the gradient on the surface a. The surface a in the current configuration r is taken as an example, though the analysis also holds for the surface $\mathscr{A}$ in the reference configuration $\mathscr{R}$. Let ξ_1 and ξ_2 be Gaussian coordinates along the directions of principal curvature of surface a, $\boldsymbol{i}_{(1)}$ and $\boldsymbol{i}_{(2)}$ be unit vectors along ξ_1 and ξ_2, and $\boldsymbol{n}$ be unit normal vector of a such that $(\boldsymbol{i}_{(1)},\boldsymbol{i}_{(2)},\boldsymbol{n})$ form a triad of orthogonal unit vectors. A tensor field $\boldsymbol{b}$ of any rank can be decomposed as

$$\boldsymbol{b} = \boldsymbol{i}_{(1)}\boldsymbol{b}_{(1)} + \boldsymbol{i}_{(2)}\boldsymbol{b}_{(2)} + \boldsymbol{n}\boldsymbol{b}_{(n)}, \tag{A.2}$$

where $\boldsymbol{b}_{(1)}$, $\boldsymbol{b}_{(2)}$ and $\boldsymbol{b}_{(n)}$ are tensor fields of rank lower by 1 than $\boldsymbol{b}$. Its last term is defined as the "normal" part $\boldsymbol{b}_n$, i.e., $\boldsymbol{b}_n = \boldsymbol{n}\boldsymbol{b}_{(n)}$, while the first two terms of the right-hand side comprise the "tangential" part $\boldsymbol{b}_t = \boldsymbol{i}_{(1)}\boldsymbol{b}_{(1)} + \boldsymbol{i}_{(2)}\boldsymbol{b}_{(2)}$ such that $\boldsymbol{n}\cdot\boldsymbol{b}_t = 0$. The gradient of $\boldsymbol{b}$ can be obtained as

$$\overset{>}{\nabla}\boldsymbol{b} = \overset{>}{\boldsymbol{D}}\boldsymbol{b} + \boldsymbol{n}\frac{\partial\boldsymbol{b}}{\partial\boldsymbol{n}}, \tag{A.3}$$

$$\begin{aligned}\overset{>}{\boldsymbol{D}}\boldsymbol{b} = {} & \overset{>}{\nabla}_S\boldsymbol{b}_t + \boldsymbol{i}_{(1)}\left[\frac{1}{R_{(1)}}\boldsymbol{i}_{(1)}\boldsymbol{b}_{(n)} + \boldsymbol{n}\left(\frac{\partial\boldsymbol{b}_{(n)}}{A_{(1)}\partial\xi_1} - \frac{1}{R_{(1)}}\boldsymbol{b}_{(1)}\right)\right] \\ & + \boldsymbol{i}_{(2)}\left[\frac{1}{R_{(2)}}\boldsymbol{i}_{(2)}\boldsymbol{b}_{(n)} + \boldsymbol{n}\left(\frac{\partial\boldsymbol{b}_{(n)}}{A_{(2)}\partial\xi_2} - \frac{1}{R_{(2)}}\boldsymbol{b}_{(2)}\right)\right],\end{aligned} \tag{A.4}$$

where $\overset{>}{\nabla}_S\boldsymbol{b}_t$ represents the terms that do not involve $\boldsymbol{n}$ or $\boldsymbol{b}_{(n)}$, and is given by

$$\begin{aligned}\overset{>}{\nabla}_S\boldsymbol{b}_t = {} & \boldsymbol{i}_{(1)}\left[\boldsymbol{i}_{(1)}\left(\frac{\partial\boldsymbol{b}_{(1)}}{A_{(1)}\partial\xi_1} + \frac{1}{A_{(1)}A_{(2)}}\frac{\partial A_{(1)}}{\partial\xi_2}\boldsymbol{b}_{(2)}\right)\right. \\ & \left. + \boldsymbol{i}_{(2)}\left(\frac{\partial\boldsymbol{b}_{(2)}}{A_{(1)}\partial\xi_1} - \frac{1}{A_{(1)}A_{(2)}}\frac{\partial A_{(1)}}{\partial\xi_2}\boldsymbol{b}_{(1)}\right)\right]\end{aligned}$$

$$+\boldsymbol{i}_{(2)}\left[\boldsymbol{i}_{(1)}\left(\frac{\partial \boldsymbol{b}_{(1)}}{A_{(2)}\partial\xi_2}-\frac{1}{A_{(1)}A_{(2)}}\frac{\partial A_{(2)}}{\partial\xi_1}\boldsymbol{b}_{(2)}\right)\right.$$

$$\left.+\ \boldsymbol{i}_{(2)}\left(\frac{\partial \boldsymbol{b}_{(2)}}{A_{(2)}\partial\xi_2}+\frac{1}{A_{(1)}A_{(2)}}\frac{\partial A_{(2)}}{\partial\xi_1}\boldsymbol{b}_{(1)}\right)\right], \tag{A.5}$$

$A_{(1)}$, $A_{(2)}$ and $R_{(1)}$, $R_{(2)}$ are Lamé parameters and principal radii of curvature of surface a, respectively. Similarly, the divergence of $\boldsymbol{b}$ can be established as

$$\overset{>}{\nabla}\cdot\boldsymbol{b}=\overset{>}{\boldsymbol{D}}\cdot\boldsymbol{b}+\boldsymbol{n}\cdot\frac{\partial \boldsymbol{b}}{\partial n},\quad \overset{>}{\boldsymbol{D}}\cdot\boldsymbol{b}=\overset{>}{\nabla}_S\cdot\boldsymbol{b}_t+\left(\frac{1}{R_{(1)}}+\frac{1}{R_{(2)}}\right)\boldsymbol{b}_{(n)}, \tag{A.6}$$

where $\overset{>}{\nabla}_S\cdot\boldsymbol{b}_t$ is the divergence of $\boldsymbol{b}_t$ within the surface and is given by

$$\overset{>}{\nabla}_S\cdot\boldsymbol{b}_t=\frac{\partial \boldsymbol{b}_{(1)}}{A_{(1)}\partial\xi_1}+\frac{\partial \boldsymbol{b}_{(2)}}{A_{(2)}\partial\xi_2}+\frac{1}{A_{(1)}A_{(2)}}\left(\frac{\partial A_{(2)}}{\partial\xi_1}\boldsymbol{b}_{(1)}+\frac{\partial A_{(1)}}{\partial\xi_2}\boldsymbol{b}_{(2)}\right). \tag{A.7}$$

The above results also hold for surface $\mathscr{A}$ in the reference configuration $\mathscr{R}$. The operators $\overset{<}{\nabla},\overset{<}{\boldsymbol{D}}$ and $\overset{<}{\nabla}_S$ are then understood to be affiliated to the Gaussian principal coordinates Ξ_1,Ξ_2 on the surface $\mathscr{A}$, with principal curvature $1/R_{(\mathrm{I})}$ and $1/R_{(\mathrm{II})}$ and Lame parameters $A_{(\mathrm{I})}$ and $A_{(\mathrm{II})}$.

The stress traction in Eq. (74) can be derived from Eq. (62) by taking $\boldsymbol{b}=\boldsymbol{n}\cdot\boldsymbol{\tau}$ in Eq. (A.6), which yields

$$\boldsymbol{t}=\boldsymbol{n}\cdot(\tilde{\boldsymbol{\sigma}}-\overset{>}{\nabla}\cdot\boldsymbol{\tau})-\overset{>}{\nabla}_S\cdot\boldsymbol{b}_t, \tag{A.8}$$

where $\boldsymbol{b}_t=\boldsymbol{b}-\boldsymbol{b}_n=\boldsymbol{n}\cdot\boldsymbol{\tau}-\boldsymbol{n}\boldsymbol{r}$. The surface divergence $\overset{>}{\nabla}_S\cdot\boldsymbol{b}_t$ in the current configuration r needs to be expressed in terms of a surface divergence in the reference configuration $\mathscr{R}$,

$$\overset{>}{\nabla}_S\cdot\boldsymbol{b}_t=\frac{1}{a_N}\overset{<}{\nabla}_S\cdot\boldsymbol{B}_T, \tag{A.9}$$

where $\boldsymbol{B}_T$, satisfying $\boldsymbol{N}\cdot\boldsymbol{B}_T=0$, is to be determined in the following.

The integration of Eq. (A.9) gives

$$\int_a\overset{>}{\nabla}_S\cdot\boldsymbol{b}_t\,\mathrm{d}a=\int_A\overset{<}{\nabla}_S\cdot\boldsymbol{B}_T\,\mathrm{d}\mathscr{A}, \tag{A.10}$$

which yields

$$\int_c\boldsymbol{k}\cdot\boldsymbol{b}_t|\mathrm{d}\boldsymbol{x}|=\int_C\mathscr{K}\cdot\boldsymbol{B}_T|\mathrm{d}\boldsymbol{X}| \tag{A.11}$$

from the surface divergence theorem, where, similar to Eq. (59), $\boldsymbol{k}$ and $\mathscr{K}$ are unit vectors normal to c and $\mathscr{C}$, lying within the tangential planes of surface a and $\mathscr{A}$, respectively. For Eq. (A.11) to hold for an arbitrary curve c, it is necessary to require $\boldsymbol{k}\cdot\boldsymbol{b}_t|\mathrm{d}\boldsymbol{x}|=\mathscr{K}\cdot\boldsymbol{B}_T|\mathrm{d}\boldsymbol{X}|$, or equivalently,

$$\boldsymbol{k}\cdot\boldsymbol{b}_t=\frac{1}{\varepsilon_{\mathscr{C}}}\mathscr{K}\cdot\boldsymbol{B}_T, \tag{A.12}$$

where $\varepsilon_{\mathscr{C}}$ is the length ratio given in Eq. (70). The substitution of $\boldsymbol{k}=\boldsymbol{c}\times\boldsymbol{n}$, $\mathscr{K}=\mathscr{C}\times\mathscr{N}$ and $\boldsymbol{b}_t=\boldsymbol{n}\cdot\boldsymbol{\tau}-\boldsymbol{n}\boldsymbol{r}$ into Eq. (A.12) leads to the equation governing $\boldsymbol{B}_T$. In conjunction

with the requirement $\boldsymbol{N} \cdot \boldsymbol{B}_T = 0$, the components of $\boldsymbol{B}_T$ can be determined and are given in Eqs. (75) and (76).

References

Acharya, A., Bassani, J.L., 2000. Lattice incompatibility and a gradient theory of crystal plasticity. J. Mech. Phys. Solids 48, 1565–1595.

Acharya, A., Beaudoi, A.J., 2000. Grain-size effect in viscoplastic polycrystals at moderate strains. J. Mech. Phys. Solids 48, 2213–2230.

Atkinson, M., 1995. Further analysis of the size effect in indentation hardness tests of some metals. J. Mater. Res. 10, 2908–2915.

Begley, M.R., Hutchinson, J.W., 1998. The mechanics of size-dependent indentation. J. Mech. Phys. Solids 46, 2049–2068.

Dai, H., Parks, D.M., 2001. Geometrically-necessary dislocation density in continuum crystal plasticity theory and FEM implementation, Unpublished manuscript.

De Guzman, M.S., Neubauer, G., Flinn, P., Nix, W.D., 1993. The role of indentation depth on the measured hardness of materials. Mater. Res. Symp. Proc. 308, 613–618.

Fleck, N.A., Hutchinson, J.W., 1993. A phenomenological theory for strain gradient effects in plasticity. J. Mech. Phys. Solids 41, 1825–1857.

Fleck, N.A., Hutchinson, J.W., 1997. Strain gradient plasticity. In: Hutchinson, J.W., Wu, T.Y. (Eds.), Advances in Applied Mechanics, Vol. 33. Academic Press, New York, pp. 295–361.

Fleck, N.A., Muller, G.M., Ashby, M.F., Hutchinson, J.W., 1994. Strain gradient plasticity: theory and experiments. Acta Metall. Mater. 42, 475–487.

Gao, H., Huang, Y., Nix, W.D., Hutchinson, J.W., 1999. Mechanism-based strain gradient plasticity—I. Theory. J. Mech. Phys. Solids 47, 1239–1263.

Huang, Y., Gao, H., Hwang, K.C., 1999. Strain-gradient plasticity at the micron scale. In: Progress in Mechanical Behavior of Materials, Ellyin, F., Provan, J.W. (Eds.), Vol. III, Fleming Printing Ltd., Victoria, BC, Canada, pp. 1051–1056.

Huang, Y., Gao, H., Nix, W.D., Hutchinson, J.W., 2000a. Mechanism-based strain gradient plasticity—II. Analysis. J. Mech. Phys. Solids 48, 99–128.

Huang, Y., Xue, Z., Gao, H., Nix, W.D., Xia, Z.C., 2000b. A study of micro-indentation hardness tests by mechanism-based strain gradient plasticity. J. Mater. Res. 15, 1786–1796.

Jiang, H., Huang, Y., Zhuang, Z., Hwang, K.C., 2001. Fracture in mechanism-based strain gradient plasticity. J. Mech. Phys. Solids, in press.

Koiter, W.T., 1964. Couple stresses in the theory of elasticity, I and II. Proc. K. Ned. Akad. Wet (B) 67, 17–44.

Lloyd, D.J., 1994. Particle reinforced aluminum and magnesium matrix composites. Int. Mater. Rev. 39, 1–23.

Ma, Q., Clarke, D.R., 1995. Size dependent hardness of silver single crystals. J. Mater. Res. 10, 853–863.

McElhaney, K.W., Vlassak, J.J., Nix, W.D., 1998. Determination of indenter tip geometry and indentation contact area for depth-sensing indentation experiments. J. Mater. Res. 13, 1300–1306.

McLean, D., 1962. Mechanical Properties of Metals. Wiley, New York.

Mindlin, R.D., 1964. Micro-structure in linear elasticity. Arch. Ration. Mech. 16, 51–78.

Mindlin, R.D., 1965. Second gradient of strain and surface tension in linear elasticity. Int. J. Solids Struct. 1, 417–438.

Nan, C.-W., Clarke, D.R., 1996. The influence of particle size and particle fracture on the elastic/plastic deformation of metal matrix composites. Acta Mater. 44, 3801–3811.

Nix, W.D., 1989. Mechanical properties of thin films. Metall. Trans. A 20A, 2217–2245.

Nix, W.D., Gao, H., 1998. Indentation size effects in crystalline materials: a law for strain gradient plasticity. J. Mech. Phys. Solids 46, 411–425.

Poole, W.J., Ashby, M.F., Fleck, N.A., 1996. Micro-hardness of annealed and work-hardened copper polycrystals. Scr. Metall. Mater. 34, 559–564.

Qiu, X., Wei, Y., Huang, Y., Gao, H., Hwang, K.C., 2001. The flow theory of mechanism-based strain gradient plasticity, submitted for publication.

Shu, J.Y., Fleck, N.A., 1998. The prediction of a size effect in micro indentation. Int. J. Solids Struct. 35, 1363–1383.

Shu, J.Y., King, W.E., Fleck, N.A., 1999. Finite elements for materials with strain gradient effects. Int. J. Numer. Methods Eng. 44, 373–391.

Stelmashenko, N.A., Walls, A.G., Brown, L.M., Milman, Y.V., 1993. Microindentation on W and Mo oriented single crystals: an STM study. Acta Metall. Mater. 41, 2855–2865.

Stolken, J.S., Evans, A.G., 1998. A microbend test method for measuring the plasticity length scale. Acta Mater. 46, 5109–5115.

Suresh, S., Nieh, T.G., Choi, B.W., 1999. Nano-indentation of copper thin films on silicon substrates. Scripta Mater. 41, 951–957.

Taylor, G.I., 1938. Plastic strain in metals. J. Inst. Met. 62, 307–324.

Toupin, R.A., 1962. Elastic materials with couple stresses. Arch. Ration. Mech. Anal. 11, 358–414.

Toupin, R.A., 1964. Theories of elasticity with couple-stress. Arch. Ration. Mech. Anal. 17, 85–112.

Wei, Y., Hutchinson, J.W., 1997. Steady-state crack growth and work of fracture for solids characterized by strain gradient plasticity. J. Mech. Phys. Solids 45, 1253–1273.

Xia, Z.C., Hutchinson, J.W., 1996. Crack tip fields in strain gradient plasticity. J. Mech. Phys. Solids 44, 1621–1648.